View metadata, citation and similar papers at core.ac.uk

brought to you by CORE

provided by Archivio istituzionale della ricerca - Università di Ferrara

Università degli studi di Ferrara

Dottorato di Ricerca in

"FISICA"

ciclo xxii

Coordinatore Prof. Filippo Frontera

Magnetic fields generated by r-modes in accreting millisecond pulsars

Settore Scientifico Disciplinare: FIS/04

Dottorando:

Dott. Carmine Cuofano

Tutore:

Dott. Alessandro Drago

Anni 2007/2009

Contents

Introduction

In rotating neutron stars the existence of the Coriolis force allows the presence of the so-called r-modes oscillations, which are similar to Rossby waves in the Earth's atmosphere and oceans. The first proposal of the r-modes in Newtonian stellar pulsation theory was advanced in a paper by Papaloizou and Pringle, in 1978 [1]. In rotating neutron stars, in the absence of damping mechanisms, r-modes become unstable due to the emission of gravitational waves by the Chandrasekhar-Friedman-Schutz (CFS) mechanism [2, 3]. Therefore, these modes play a very important role in the astrophysics of rapidly rotating compact stars and in the search for gravitational waves. In particular the r-mode instability may play a role in the evolution of the fastest spinning pulsars, and they may be presently active in the rapidly spinning neutron stars observed in Low Mass X-Ray Binaries (LMXBs). This scenario can provide an explanation for the sub-breakup spin rates of both LMXBs and of young, hot neutron stars.

The possibility that the rotation of recycled pulsars may be limited by the emission of gravitational radiation is interesting because the gravitational waves, from a neutron star unstable with respect to r-modes, may be detectable with the new generation of interferometric detectors.

Another important point concerns the possibility to investigate through r-modes

the physics and the composition of the inner regions of compact stars. Indeed, a significant damping mechanism of the r-mode instability is provided by viscosity, either shear or bulk, that depends critically on temperature and composition of the star. This condition provide a link between spin frequency, spin down rate, temperature and internal composition of the star, that is possible to investigate making use of the observational data about the fastest spinning pulsars.
R-mode instability is also associated with kinematical secular effects which generate differential rotation in the star and large scale mass drifts, particularly in the azimuthal direction. Differential rotation in turn can produce very strong toroidal magnetic fields inside the star and these fields damp instabilities converting the energy of the mode into magnetic energy.
This scenario was investigated in [4, 5, 6] in the case of young, rapidly rotating neutron stars. It was shown that, in these objects, the r-mode instability can generate huge magnetic fields, thus opening new interesting possibilities in the investigation of some astrophysical phenomena, e.g. the generation of Gamma Ray Bursts (GRBs).

In the Thesis I concentrate on the interaction between magnetic field and r-modes in the core of accreting neutron stars. I consider the back-reaction of the magnetic fields on r-mode instabilities by inserting for the first time the magnetic damping rate into the evolution equations of r-modes. In this way we can follow the temporal evolution of both magnetic fields and r-modes even on a long time scale.
In particular I investigate two astrophysical scenarios:

- Stabilization with respect to r-modes of neutron stars *accelerated to mil-*

lisecond spin period by accretion of matter: above few hundreds Hertz the viscosity is not able to stabilize further the star with respect to r-modes; without other damping mechanisms, the star spins down by emission of gravitational waves; I show how the development of the r-mode instabilities can generate very strong magnetic fields in accreting millisecond pulsars, and how these fields can stabilize the star at higher spin frequencies.

- Spin frequency evolution of the rapidly rotating neutron stars in LMXBs *when the accretion of matter stops*: I show how, in our scenario, the diffusion of the generated internal magnetic field can induce a new development of the r-mode instability that in turn can influence the spin down of the fastest spinning pulsars; our conclusions can be important to better understand the claimed connection between LMXBs and Radio Millisecond Pulsars (MSPs).

The structure of the Thesis is the following: in Chapter 1 I give an overview of the r-modes and of the related open problems; in Chapter 2 I discuss the interaction between r-modes and magnetic fields and I obtain a new evolution equations of r-modes, introducing a new term associates with the magnetic damping; in Chapter 3 I make use of these new equations to investigate the generation of huge magnetic fields in accreting millisecond pulsars, putting particular attention on the stabilization of the r-mode instability by the new generated magnetic fields; in Chapter 4 I investigate how the r-mode instability, driven by the diffusion of the internal magnetic fields, can influence the spin frequency evolution of accreting and of old, isolated millisecond pulsars. Finally, I will summarize the results and discuss future extension of the work in the Conclusion and Outkook.

List of publications

The work presented in this Thesis is based on the following papers and preprints:

- "Magnetic fields generated by r-modes in accreting millisecond pulsars".
  Carmine Cuofano and Alessandro Drago.
  Journal of Physics Conference Series 168 (2009) 012008.

- "Magnetic fields generated by r-modes in accreting millisecond pulsars".
  Carmine Cuofano and Alessandro Drago.
  Submitted for publication.

Chapter 1

R-mode instability in rotating neutron stars

R-modes are axial perturbations and represent large scale oscillating currents that move approximately along the equipotential surfaces of the rotating star. The restoring force for these oscillations is the Coriolis force. In neutron stars, the r-modes play a very important role because they are unstable due to emission of gravitational waves by the Chandrasekhar-Friedman-Schutz (CFS) mechanism [2, 3].

In the following we give a general overview about the r-mode instability in neutron stars, focusing on the damping effect due to the viscosity. In the end we rapidly discuss how the presence of a rigid crust or hyperons and quarks in the nucleus can influence the development of this instability.

1.1 The CFS mechanism

The first proposal that rotating neutron stars are generically unstable due to the emission of gravitational waves was advanced by Chandrasekhar considering the Maclaurin spheroids to represent a rotating star [7]. Subsequently Friedman and Schutz proved that the instability is generic and all rotating fluid neutron star are unstable [8, 9, 10].

To understand the mechanism for gravitational-wave instability, it is possible to represent the problem in the following way. In spherical stars, gravitational radiation removes positive angular momentum from a mode moving in the same direction of the star and negative angular momentum from a backward-moving mode; it therefore damps all time-dependent nonaxisymmetric modes [3]. Once the angular velocity of the star is sufficiently large, however, a mode that moves backward relative to the star is dragged forward relative to an inertial observer. Gravitational radiation will then remove positive angular momentum from the mode. But a mode that moves backwards relative to the fluid has negative angular momentum, because the perturbed fluid does not rotate as fast it did without the perturbation. The radiation thus removes positive angular momentum from a mode whose angular momentum is negative. By making the angular momentum of the perturbation increasingly negative, gravitational radiation drives the mode. This class of frame-dragging instabilities is usually refered to as Chandrasekhar-Friedman-Schutz (CFS) instabilities.

The fact that the emission of gravitational radiation causes a growth in the mode energy in the rotating frame E_r, despite the decrease in the inertial frame energy E_i, can be understood from the relation between the two energies: $E_r = E_i - \Omega J$, where Ω is the angular velocity of the star and J is the total angular momentum

of the star. From this we see that E_r may increase even if both E_i and J are both decreasing. In other words, when the mode radiates away angular momentum the star can find a rotational state of lower angular momentum and lower energy. Under these conditions the mode amplitude may grow.

Stability is governed by the sign of the canonical energy E_c, when expressed in terms of canonical displacements ξ [8]. A star model is unstable to perturbations with angular dependence $e^{i\sigma t}$ when $E_c(\xi) < 0$. In a Newtonian star, the canonical energy evaluated to order Ω^2 has the form [3]

$$E_c = -\frac{1}{2}\int dV \rho |\xi|^2 \left[(m\Omega - \sigma)(m\Omega + \sigma) - \frac{2m}{2m+1}\Omega^2\right] \tag{1.1}$$

where

$$\sigma = \frac{2m\Omega}{l(l+1)} - m\Omega \tag{1.2}$$

is the angular frequency of the mode in the inertial frame [1].

If E_c is negative and the system (the star) is coupled to another system (the radiation) in such a way E_c must decrease with time, then the absolute value of E_c will increase and the associated mode is unstable.

From the relation involving also the canonical angular momentum J_c [11]

$$J_c = \frac{E_c}{\sigma} \tag{1.3}$$

which is a general property of linear waves, follows that the condition $E_c < 0$ is equivalent to the simple notion of a retrograde mode being dragged forwards.

1.2 The r-mode instability

We will focus our discussion on the gravitational-wave driven instability of the so-called r-modes.

Since these modes are prograde in the inertial frame and retrograde in the co-rotating frame, they satisfy the Newtonian criterion for the CFS instability. Hence, one can easily deduce that the r-modes ought to be unstable. That this instability is generic also in the relativistic case was first shown by Friedman and Morsink [3]. In perfect fluid stars the r-modes are unstable at all rates of rotation. For real stars the stability of the r-modes depends on the competing influences of gravitational radiation reaction (that drives the mode), viscous and magnetic damping.

The r-modes of rotating Newtonian stars are generally defined to be solutions of the perturbed fluid equations having Eulerian velocity perturbations of the form

$$\delta\vec{v} = R\Omega f(r/R)\vec{Y}^B_{lm}e^{i\sigma t} \tag{1.4}$$

where R and Ω are the radius and the angular velocity of the unperturbed star, $f(r/R)$ is an arbitrary dimensionless function and $\vec{Y}^B_{lm}$ is the magnetic vector spherical harmonic defined by

$$\vec{Y}^B_{lm} = [l(l+1)]^{-1/2} r\vec{\nabla} \times (r\vec{\nabla}Y_{lm}) \ . \tag{1.5}$$

For barotropic stellar models $f(r/R) = \alpha(r/R)^l$, where α is a dimensionless coefficient that describes the amplitude of the perturbation. These modes exist with velocity perturbation as given by Eq. (1.4) if and only if $l = m$ [12]. The frequency of these modes in the inertial frame can be obtained using Eq.(1.2)

$$\sigma = -\frac{(l-1)(l+2)}{l+1}\Omega \ . \tag{1.6}$$

These expressions for $\delta\vec{v}$ and σ are the lowest order terms in an expansion in terms of the angular velocity Ω. The exact expression contain additional terms of order Ω^3.

The r-modes evolve with a time dependence $e^{i\sigma t - t/\tau}$ as a consequence of ordinary hydrodynamics and the influence of the various dissipative processes. The imaginary part $1/\tau$ of the frequency of these modes ω is determined by the effects of gravitational radiation, viscosity, magnetic field, etc.

The time derivative of the energy of the mode $\tilde{E}$ is related to the imaginary part of the frequency $1/\tau$ by

$$\frac{d\tilde{E}}{dt} = -\frac{2\tilde{E}}{\tau}\,. \tag{1.7}$$

The lowest order expression for the energy of the mode $\tilde{E}$, as measured in the corotating frame, reads [13]

$$\tilde{E} = \frac{1}{2}\alpha^2\Omega^2 R^{-2l+2}\int_0^R \rho r^{2l+2} dr\,. \tag{1.8}$$

We will make use of Eqs. (1.7,1.8) to evaluate the stability of r-modes.

1.2.1 Gravitational radiation reaction

The gravitational radiation tends to increase the energy of r-modes making them unstable at all rates of rotation. The lowest order contribution to the gravitational radiation term in the energy dissipation comes from the current multipole moment δJ_{ll} that at lowest order in Ω is [13]

$$\delta J_{ll} = \frac{2\alpha\Omega}{cR^{l-1}}\sqrt{\frac{l}{l+1}}\int_0^R \rho r^{2l+2} dr\,. \tag{1.9}$$

Higher multipoles lead to significantly weaker instabilities and the $l = m = 2$ r-mode will be the most important.

The variation of the r-mode energy due to the gravitational radiation is

$$\left(\frac{d\tilde{E}}{dt}\right)_{GR} \approx -\omega^{2l+1} N_l |\delta J_{lm}|^2 \tag{1.10}$$

where N_l is the coupling constant between the gravitational radiation and the evolution of the mode through the current multipole moment of the perturbed fluid

$$N_l = \frac{4\pi G}{c^{2l+1}} \frac{(l+1)(l+2)}{l(l-1)[(2l+1)!!]^2} \,. \tag{1.11}$$

The gravitational radiation growth rate $F_g \equiv -1/\tau_g$ can be obtained using Eq.(1.7)

$$F_g = \frac{1}{2\tilde{E}} \left(\frac{d\tilde{E}}{dt} \right)_{GR} \,. \tag{1.12}$$

It is possible to obtain an explicit expression for the gravitational radiation growth rate by using Eqs. (1.8),(1.10) and (1.12)

$$F_g = \frac{32\pi G\Omega^{2l+2}}{c^{2l+3}} \frac{(l-1)^{2l}}{[(2l+1)!!]^2} \left(\frac{l+2}{l+1} \right)^{2l+2} \times \int_0^R \rho r^{2l+2} dr \tag{1.13}$$

In our numerical analysis we make use of the estimate given in Ref. [11] for the gravitational radiation reaction rate due to the $l = m = 2$ current multipole

$$F_g = \frac{1}{47} M_{1.4} R_{10}^4 P_{-3}^{-6} \quad \mathrm{s}^{-1} \tag{1.14}$$

where we have used the notation $M_{1.4} = M/1.4\ M_\odot$, $R_{10} = R/10$ Km, $P_{-3} = P/1$ ms and $T_9 = T/10^9$ K.

1.2.2 Viscous damping

In our neutron star models we considered two kinds of viscosity, bulk and shear, that are due to rather different physical mechanisms. We discuss them separately below.

Shear viscosity

The shear viscosity is related to the momentum transport due to particle scattering, and in a fluid star it is the main viscous dissipation mechanism at temperature below few times 10^9 K. In a normal fluid star the most important contribution derive from the neutron-neutron scattering. In a superfluid star the dominant contribution is due to the electron-electron scattering but the estimate is more complicate and uncertain, because it is necessary to take into account other exotic effects, like the scattering of vortices in the superfluid.
The shear viscosity damping rate, $F_{sv} \equiv 1/\tau_{sv}$, reads [13]

$$F_{sv} = (l-1)(2l+1)\int_0^R \eta r^{2l} dr \left(\int_0^R \rho r^{2l+2} dr\right)^{-1} \tag{1.15}$$

where η is the shear viscosity.
We will make use of the numerical estimate given in Ref. [11] obtained for a star that has cooled below the superfluid transition temperature of $\sim 10^9$ K

$$F_{sv} \approx \frac{1}{2.2\times 10^7} M_{1.4} R_{10}^{-5} T_9^{-2} \quad \mathrm{s}^{-1} \tag{1.16}$$

Bulk viscosity

The bulk viscosity is related to the departure from beta equilibrium due to the variations of density and pressure associated with the mode oscillations. It corresponds to an estimate of the extent to which energy is dissipated from the fluid motion as the weak interaction tries to re-establish equilibrium. The energy of the mode is carried away by neutrinos. The bulk viscosity is the dominant viscous mechanism at temperature above a few times 10^9 K.

The bulk viscosity damping rate, $F_{bv} \equiv 1/\tau_{bv}$, reads [13]

$$F_{bv} \approx \frac{4R^{2l-2}}{(l+1)^2} \int \varsigma |\frac{\delta\rho}{\rho}| d^3x \left(\int_0^R \rho r^{2l+2} dr \right)^{-1} \tag{1.17}$$

where ς is the bulk viscosity.

In our numerical calculation we make use of the numerical estimate given in Ref. [14]

$$F_{bv} = \frac{1}{6.99 \times 10^8} \left(\frac{T}{10^9 K} \right)^6 \left(\frac{\Omega^2}{\pi G \bar{\rho}} \right) \tag{1.18}$$

which we can approximately rewrite as

$$F_{bv} = \frac{1}{2.5 \times 10^9} M_{1.4}^{-1} R_{10}^3 P_{-3}^{-2} T_9^6 \quad \mathrm{s}^{-1} \, . \tag{1.19}$$

1.2.3 Temperature evolution

Viscosity depends critically on temperature. We include three factors in modeling the temperature evolution: modified Urca cooling, shear viscosity reheating and accretion heating. The cooling rate due to the modified Urca reactions, $\dot{\epsilon}_u$, reads [15]

$$\dot{\epsilon}_u = 7.5 \times 10^{39} M_{1.4}^{2/3} T_9^8 \quad \mathrm{erg\ s}^{-1} \, . \tag{1.20}$$

It is important to remark that if direct Urca processes can take place they deeply influence the cooling rate, which becomes significantly larger [16]. The bulk viscosity is also enhanced at temperatures smaller than $\sim 2 \times 10^9$ K [17]. A recent phenomenological analysis of the implications of the direct Urca processes can be found e.g. in [18]. In our analysis we have assumed for simplicity that only modified Urca processes can take place.

The neutron star will be heated by the action of shear viscosity on the r-mode

oscillations. The heating rate due to shear viscosity, $\dot{\epsilon}_s$, reads [11]

$$\begin{aligned} \dot{\epsilon}_s &= 2\alpha^2\Omega^2 MR^2\tilde{J}F_s \\ &= 8.3\times10^{37}\alpha^2\Omega^2\tilde{J}M_{1.4}^{9/4}R_{10}^{-15/4}T_9^{-2} \quad \text{erg s}^{-1}\,. \end{aligned} \tag{1.21}$$

where $\tilde{J}=1.635\times10^{-2}$.

Accretion heating has two components. We use the estimates given in [19]. The first contribution arises when accreted matter undergoes nuclear burning at the surface of the star

$$\dot{\epsilon}_n = \frac{\dot{M}}{m_B}\times 1.5 \text{ MeV} = 4\times10^{51}\dot{M}_{1.4} \quad \text{erg s}^{-1} \tag{1.22}$$

where m_N is the mass of a nucleon and $\dot{M}_{1.4}=\dot{M}/1.4M_\odot$ is measured in s^{-1}.

The second contribution arises because the flow is assumed to be advection dominated. The advected potential energy is used to generate neutrinos near the surface of the star. Half of these neutrinos are radiated into the star, where they scatter and interact with the stellar material. The heating rate is

$$\dot{\epsilon}_h \sim \frac{R}{\lambda}\frac{GM\dot{M}}{R} = 8\times10^{51}M_{1.4}^{13/6}\dot{M}_{1.4} \quad \text{erg s}^{-1} \tag{1.23}$$

where λ is the mean free path of inelastic scattering of neutrinos [19]. Notice that if the advection related contribution is negligible, the temperature at which the star enters the instability region is lower and, as we show in the following, the generated toroidal magnetic fields are larger.

Finally we use the estimate of the heat capacity C_v also given in [19]

$$C_v = 1.6\times10^{39}M_{1.4}^{1/3}T_9 \quad \text{erg K}^{-1}. \tag{1.24}$$

The equation of thermal balance of the star reads therefore

$$\frac{d}{dt}\left[\frac{1}{2}C_vT\right] = \dot{\epsilon}_s - \dot{\epsilon}_u + \dot{\epsilon}_n + \dot{\epsilon}_h\ . \tag{1.25}$$

1.3 R-mode equations

In this section we obtain the evolution equations of r-modes by considering only bulk and shear viscosity as damping mechanisms. In order to derive the equations regulating the evolution of r-modes we start by considering the conservation of angular momentum, following Ref. [20]. The total angular momentum J of a star can be decomposed into an equilibrium angular momentum J_* and a canonical angular momentum J_c proportional to the r-mode perturbation:

$$J = J_*(M, \Omega) + (1 - K_j)J_c, \qquad J_c = -K_c\alpha^2 J_* \tag{1.26}$$

where $K_{(j,c)}$ are dimensionless constants and $J_* \cong I_*\Omega$.
Following Ref. [9] the canonical angular momentum obeys the following equation:

$$dJ_c/dt = 2J_c\{F_g(M, \Omega) - [F_v(M, \Omega, T_v) + N_{other}]\} \tag{1.27}$$

where F_g is the gravitational radiation growth rate, $F_v = F_s + F_b$ is the sum of the shear and bulk viscous damping rate, $T_v(t)$ is a spatially averaged temperature and N_{other} is the torque associated with other processes that can drive the mode. The total angular momentum satisfies the equation:

$$dJ/dt = 2J_cF_g + \dot{J}_a(t) - I_*\Omega F_{m_e} \tag{1.28}$$

where $\dot{J}_a$ is the rate of accretion of angular momentum (we have assumed it to be $\dot{J}_a = \dot{M}(GMR)^{1/2}$, see Ref. [21]) and F_{m_e} is the magnetic breaking rate associated to the external poloidal magnetic field. Combining Eqs. (1.27) and (1.28) we obtain the evolution equations of the r-mode amplitude α and of the

angular velocity of the star Ω:

$$\begin{aligned}\frac{d\alpha}{dt} &= \alpha(F_g - F_v) + \alpha[K_j F_g + (1-K_j)F_v]K_c\alpha^2 \\ &- \frac{\alpha\dot{M}}{2\tilde{I}\Omega}\left(\frac{G}{MR^3}\right)^{1/2} + \frac{\alpha F_{m_e}}{2} \qquad (1.29)\\ \frac{d\Omega}{dt} &= -2K_c\Omega\alpha^2[K_j F_g + (1-K_j)F_v] \\ &- \frac{\dot{M}\Omega}{M} + \frac{\dot{M}}{\tilde{I}}\left(\frac{G}{MR^3}\right)^{1/2} - \Omega F_{m_e} \qquad (1.30)\end{aligned}$$

where $I_* = \tilde{I}MR^2$ with $\tilde{I} = 0.261$ for an n=1 polytrope and $K_c = 9.4 \times 10^{-2}$, see Ref. [14]. Our results turn out to be rather insensitive to the value of $K_j \sim 1$ (see Ref. [20]).

When the star enters the instability region, at first an unstable r-mode grows exponentially, but soon it may enter a regime where other inertial modes that couple to r-mode become excited and nonlinear effects become important [22]. These nonlinear effects are crucial in determining the final saturation amplitude α_s of the r-mode.

In the following we solve numerically Eqs.(1.29,1.30) and in Cap. 3 we make use of these results to put in evidence how this scenario changes by taking into account the internal magnetic field.

1.4 The r-mode instability window

In the simplest scenario of the r-mode instability, which is the one typically discussed in the literature, it is considered only the damping effects due to viscosity. To have an instability it is necessary that the gravitational radiation growth rate

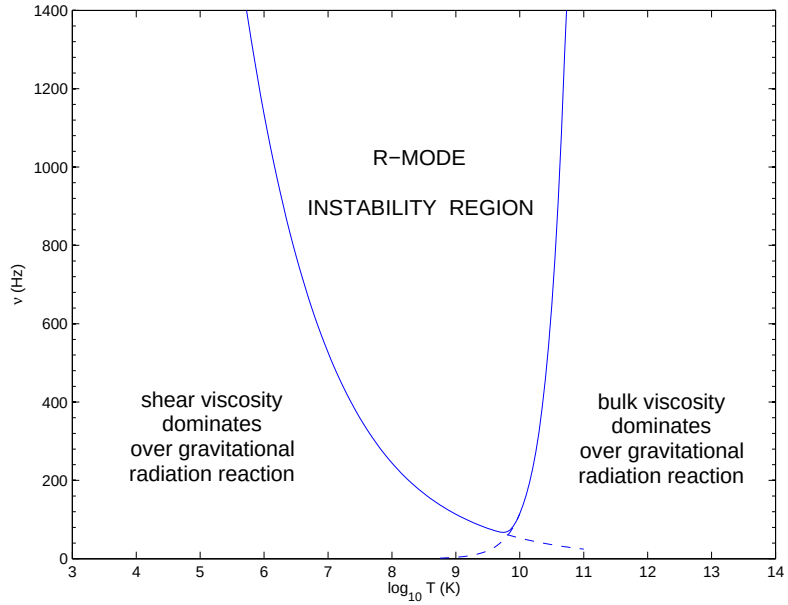

Figure 1.1: R-mode instability region in the plane $T - \nu$, obtained by using Eqs. (1.16,1.18). The solid line is the critical rotation rate of a neutron star and it has been obtained by solving Eq. (1.31).

F_g exceeded the viscous damping rate $F_v \equiv F_{sv} + F_{bv}$. A critical rotation rate for a star is obtained by solving the equation

$$F_g - F_v = 0\,. \tag{1.31}$$

The solutions of Eq.(1.31), using Eqs.(1.16,1.18), determine the r-mode instability region in a $T - \nu$ plane, see Fig.(1.1). With reference to Fig (1.1), in the region below the solid line the star is stabilized with respect to the r-modes by the viscous damping. At lower temperature $T \lesssim 10^9$ K, the shear viscosity dominates and stabilize the star at all spin frequencies for $T \lesssim 10^6$ K. Bulk viscosity instead

dominates at higher temperature $T \gtrsim 10^{10}$ K, and stabilize the star at all spin frequencies for $T \gtrsim 10^{11}$ K.

In the region above the solid line, the gravitational radiation growth rate exceeds the viscous damping rate. When this condition is verified, the r-mode instability is free to develop and the star spins down by emission of gravitational waves. Therefore the r-mode instability region, showed in Fig (1.1), should be precluded to rapidly rotating neutron stars.

Clearly these results must be combined with the condition that a stable star can never spin faster than the rate at which matter is ejected from the equator. Fully relativistic calculations for stellar models obtained using realistic equations of state suggest a Keplerian limit [23, 24]

$$\nu_K \approx 0.12\sqrt{\pi G\bar{\rho}} \tag{1.32}$$

where G is the gravitational constant and $\bar{\rho}$ is the average density of the corresponding nonrotating star.

In the next section we analyze how the existence of the r-mode instability region can influence the evolution of the spin frequency of rapidly rotating compact stars.

1.5 The spin evolution of millisecond pulsars

In this Section we discuss the spin evolution of accreting and of newly born neutron stars that enter the r-mode instability region, obtained by solving numerically Eqs.(1.29,1.30). Here we assume that r-modes are damped only by the viscous damping. We will make use of these results to emphasize in the following

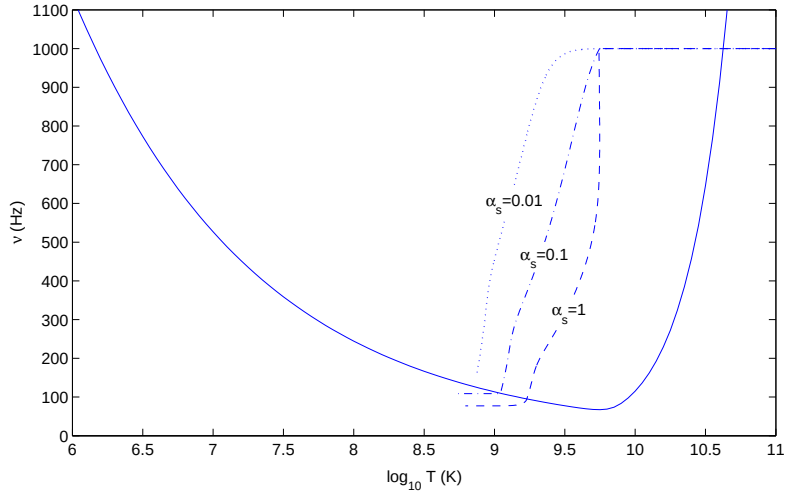

Figure 1.2: Trajectory of newly born neutron star in the Temperature vs Frequency plane. We plot three different curves corresponding to three values of the saturation amplitude of the r-modes: $\alpha_s = 1$ (dashed line), $\alpha_s = 0.1$ (dashed-dotted line) and $\alpha_s = 0.01$ (dotted line).

how this "canonical" scenario change substantially by taking into account the internal magnetic fields.

Newly born neutron stars

A hot ($T \sim 10^{11}$ K) newly born compact star rotating at millisecond period, enters the instability region, from the right side, few minutes after its formation. The trajectory of the star in the instability region depends on the saturation value of the r-mode amplitude α_s, see Fig. 1.2. Once entered the r-mode instability region, the star loses in few years much of its initial angular momentum by emission of gravitational waves. It is clear that in this scenario it should be very difficult to observe a newly born neutron star rotating at frequencies above few hundreds

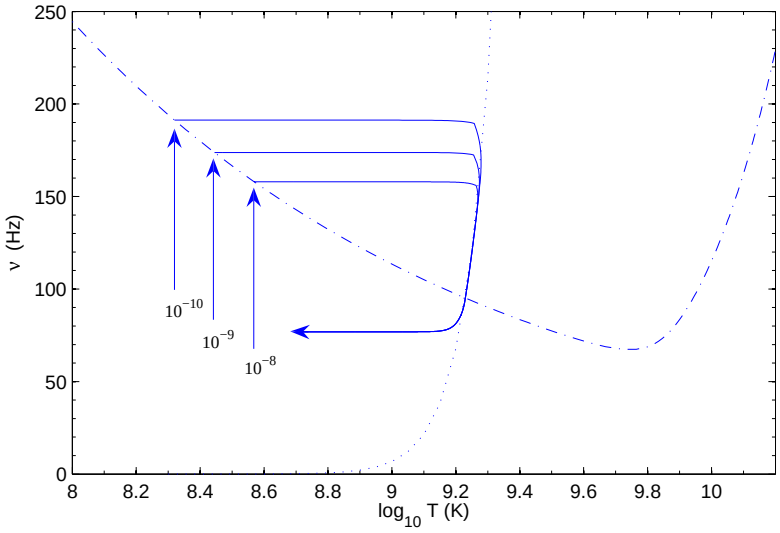

Figure 1.3: Trajectories followed by accreting neutron stars (solid lines) in the Temperature vs Frequency plane. The three curves correspond to different values of accretion rate $\dot{M} = (10^{-8}, 10^{-9}, 10^{-10})\,\mathrm{M}_{\odot}\mathrm{yr}^{-1}$. We plot also the temperature equilibrium curve (dotted line), obtained taking into account the neutrino cooling and the reheating due to viscosity. Here we have assumed $\alpha_s = 1$.

Hertz.

Accreting neutron stars

Accreting neutron stars reach the instability region from the bottom, at temperatures in the range 10^8–10^9 K, see Fig. 1.3. When the r-modes develop, the star is heated by the viscosity and spins down by emission of gravitational waves. In the instability region the star follows the trajectories showed in Fig. 1.3. In a time between a few years and a few hundreds of years, whose value strongly depends on the value of the saturation amplitude α_s, the star moves out of the instability

region and it is again stabilized by viscosity. After that the star cools down by neutrino emission in millions of years. This cycle could repeat several times until mass accretion is active.
In this scenario it should be impossible to accelerate a initially slowly rotating neutron star up to frequencies of about 200 Hz.

It is clear that in the absence of damping mechanisms other than viscosity, it should be impossible to have neutron stars with spin frequencies above few hundreds Hertz. This is in contrast with the observational data about the millisecond pulsars in Low Mass X-Ray Binaries systems (LMXBs) with spin frequencies above 600 Hz and temperature in the range 10^8–10^9 K. In the next section we analyze this problem providing a short description of more complex models involving the presence of a rigid crust or quark and hyperon in the core of compact stars.

1.6 Open Problems

Accreting millisecond pulsars in LMXBs appear to have a sort of upper limit corresponding to a spin frequency at ~ 600 Hz. The r-mode instability has been proposed as an explanation for the sub-breakup spin rates of both LMXBs and of young, hot neutron stars [25]. The idea that gravitational radiation could balance accretion was proposed independently by Bildsten [26] and Andersson et al. [25]. It is evident that the scenario in which the viscosity of a pure fluid neutron star is the only damping mechanism for the r-mode instability is too simple and it is not adequate to explain the phenomenology of the millisecond

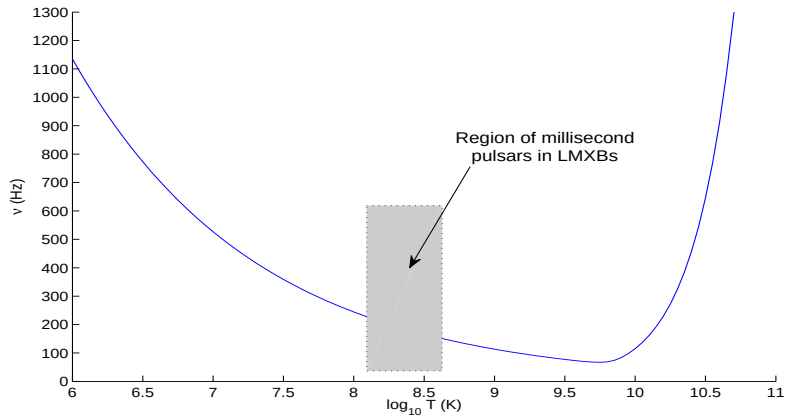

Figure 1.4: We show the region occupied by millisecond neutron stars in LMXBs in the T–ν plane (gray zone). It is evident that others damping mechanisms than viscosity are necessary to stabilize the compact stars with respect to r-modes up to frequencies $\nu > 600$ Hz.

pulsars. Indeed, accreting millisecond pulsars in LMXBs could not rotate at frequency above ~ 200 Hz because they would become unstable with respect to r-modes, see Fig.1.4.

In the last years several authors [22, 27, 28, 29, 30, 31] analyzed how a rigid crust or the presence of hyperons and quarks in the core of neutron star could modify the r-mode instability region.

Anyway it is very difficult to give a precise estimate of these effects and in our analysis we have not included them in order to study in more clear way the effects of magnetic fields on r-mode instability. In the following we shortly discuss the Ekman layer and hybrid and quark stars.

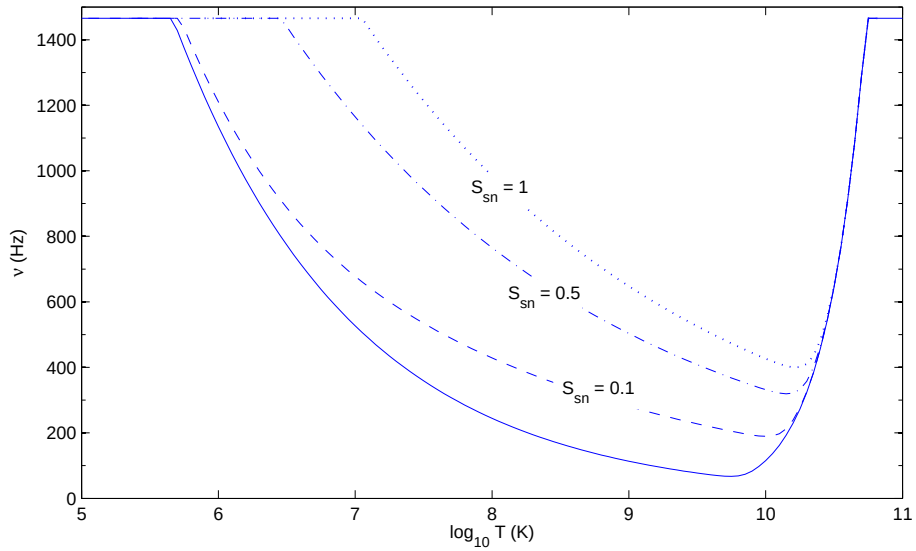

Figure 1.5: We show how change the r-mode instability window in the presence of the Ekman layer. We plot three curve corresponding to three values of the slippage factor ($\mathcal{S}_{sn} = 0.1, 0.5, 1$).

Ekman Layer

A crust may form shortly after the neutron star birth, at temperatures below $T \sim 10^{10}$ K. The effect of a crust is to increase significantly the friction with respect to a purely fluid neutron star and therefore to reduce the instability region. If the crust is assumed to be rigid, the fluid motion must essentially fall off to zero at the base of the crust in order to satisfy a no-slip condition in the rotating frame of reference. The region immediately beneath the crust corresponds to the so-called Ekman layer. For typical parameters of rapidly rotating neutron stars, this layer should have a thickness of few centimeters [11].

A precise estimate about the dissipation timescale due to the presence of the Ekman layer is difficult to obtain because it is dependent on uncertain parameters,

such as the thickness of the crust and the degree of pinning of the vortices in the crust. Recent estimates [22] about this boundary layer viscosity, give a maximum stable spin frequency for accreting neutron stars

$$\nu_{max} \approx 800 Hz \, [\mathcal{S}_{ns}/(M_{1.4}R_6)]^{4/11} T_8^{-2/11} \tag{1.33}$$

where $\mathcal{S}_{sn}$ is the slippage factor [20]

$$\mathcal{S}_{ns} = \left(\frac{2\mathcal{S}_n^2 + \mathcal{S}_s^2}{3} \right)^{1/2} . \tag{1.34}$$

$\mathcal{S}_s$ is the fractional degree of pinning of the vortices in the crust while $\mathcal{S}_n$ is the fractional difference in velocity of the normal fluid between the crust and the core. In Fig. (1.5) we show how the r-mode instability window change by changing the slippage factor $\mathcal{S}_{ns}$. It is clear that the stabilization of the faster millisecond pulsars require a large boundary layer viscosity with $\mathcal{S}_{ns} \sim 1$.

Hybrid and quark stars

As was pointed out in Ref. [32], the r-mode instability may provide the means for distinguishing between strange stars and neutron stars. The main reason for this is that the viscosity coefficients are rather different in the two cases. While the shear viscosity in a strange star is comparable to that of a neutron star, the bulk viscosity is many orders of magnitude stronger than its neutron star counterpart. This has interesting effects on the r-mode instability.

The shear viscosity damping rate in a hybrid/quark star is [11]

$$F_{sv} = \frac{1}{7.4 \times 10^7} \left(\frac{0.1}{\alpha_s} \right)^{5/3} M_{1.4}^{5/9} R_{10}^{-11/3} T_9^{-5/3} \tag{1.35}$$

where α_s is the fine-structure constant for the strong interaction.

The estimates for the bulk viscosity, which is now a result of the change in

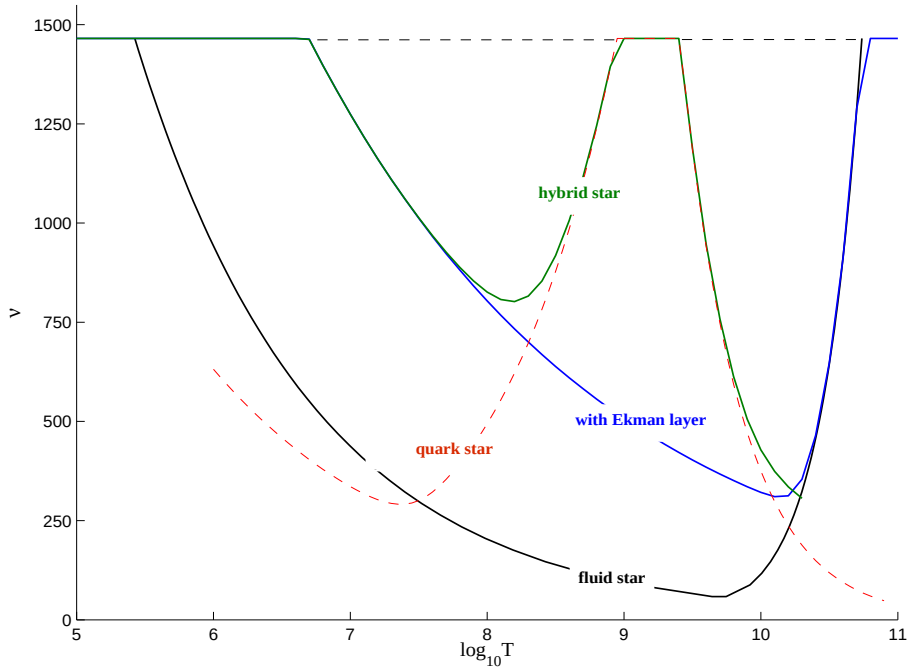

Figure 1.6: R-mode instability window in quark (dashed red line) and hybrid stars (green line). The unstable region splits in two parts: a High Temperature Instability Window (HTIW) and a Low Temperature Instability Window (LTIW). As comparison we show also the r-mode instability window for normal fluid stars (solid black line) and the r-mode instability window in the presence of the Ekman layer (blue line).

concentration of down and strange quarks in response to the mode oscillation, are more complicated. The relevant viscosity coefficient takes the form [32]

$$\varsigma = \frac{\alpha T^2}{[(k\Omega)^2 + \beta T^4]} \tag{1.36}$$

with the coefficient α and β given in [33]. From this relation we can deduce that the bulk viscosity becomes less important at both very low and very high temperature. For low temperature the bulk viscosity damping rate reads [11]

$$F_{bv}^{low} \approx \frac{1}{7.9}\, M_{1.4}^{-2} R_{10}^{4} P_{-3}^{-2} T_9^2 m_{100}^4\, s^{-1} \tag{1.37}$$

where m_{100} represents the mass of the strange quark in units of 100 MeV.
For high temperature the bulk viscosity damping rate reads [32]

$$F_{bv}^{high} \approx \frac{1}{0.268} \left(\frac{\Omega^2}{\pi G \bar{\rho}}\right)^2 T_9^{-2} m_{100}^4\, s^{-1}\,. \tag{1.38}$$

In Fig. 1.6 we show how the r-mode instability window changes for quark and hybrid stars. Due to the bulk viscosity, the instability window splits into two parts: one which starts at temperatures larger than few times 10^9 K (HTIW) and a lower temperature window at temperature smaller than 10^9 K (LTIW). The HTIW does not affect significantly the angular velocity of the star because the cooling of a newly born star is so fast that there is not enough time for the r-mode instability to drag a significant fraction of the angular momentum. Therefore, the star exits the HTIW with an angular velocity close to the initial one [30]. When the temperature drops down to a few 10^8 K the star reaches the LTIW and it starts to lose angular momentum due to r-mode instability.

All the models that we have discussed do not consider the interaction between

r-modes and the internal magnetic field of the star. In the following we take into account this effect for a normal neutron star without a crust and we investigate how the generation of huge internal fields, due to the differential rotation induced by r-modes, modify the condition for the development of the instability.

Chapter 2

R-mode instability and magnetic field

R-mode instabilities are associated with kinematical secular effects which generate differential rotation in the star and large scale mass drifts, particularly in the azimuthal direction. Differential rotation in turn can produce very strong toroidal magnetic fields inside the star and these fields damp instabilities converting the energy of the mode into magnetic energy. This mechanism has been proposed in the case of rapidly rotating, isolated and newly born neutron stars in Refs. [4, 5, 6, 34].

The high electrical conductivity in the core of neutron stars determines that the magnetic field is predominantly advected with the fluid. When the electrical conductivity is infinite (the ideal magnetohydrodynamical limit), magnetic field lines are frozen in the fluid and move entirely with it. As pointed out in Ref. [34], the generation of magnetic fields under these circumstance can be very efficient and extremely intense magnetic fields can be created during the instability. Since

the normal modes of the star are global in character, the effects of a magnetic field cannot be fully analyzed by a local analysis, such as one done by making a local comparison of forces [5, 6]. In the following we will consider a mode-energy approach, that takes into account the global properties of the modes and of the magnetic field.

If there is not enough energy in the mode to supply the magnetic energy increase required to complete an oscillation, a "full" r-mode oscillation will not occur. Stated differently, if the magnetic field exceeds a critical value, $B_{crit,p}$, the magnetic stress that builds up during an oscillation will be so large that it will halt the fluid motion involved in the oscillation. The condition that defines $B_{crit,p}$ is therefore

$$\delta E_M = \tilde{E}\,, \tag{2.1}$$

where $\tilde{E}$ is the energy of the mode in the corotating frame (see Eq. 1.8), that for $l = m = 2$ reads

$$\tilde{E} = \frac{1}{2}\frac{\alpha^2\Omega^2}{R^2}\int_0^R \rho r^6 dr \simeq 8.2\times 10^{-3}\alpha^2 M\Omega^2 R^2\,, \tag{2.2}$$

and δE_M is the change in magnetic energy density

$$\delta E_M \equiv \frac{1}{8\pi}\int_{V_\infty} \delta B^2 d^3x \tag{2.3}$$

with $\delta B^2 = (\delta B^p)^2 + (\delta B^\phi)^2$.

In the following we will make use of Eqs. (2.2,2.3) to calculate both the value of the toroidal field generated by r-modes and the magnetic damping rate, F_{m_i}, that we will introduce for the first time in the equations regulating the evolution of the r-modes. These new equations will be used in Chapter 3 to analyze the evolution of accreting millisecond pulsars.

2.1 Distorsion of the stellar magnetic field

While the star remains in the instability region, the r-modes generate a differential rotation which can greatly amplify a pre-existent magnetic field. More specifically, if a poloidal magnetic field was originally present, a strong toroidal field is generated inside the star. The energy of the modes is therefore transferred to the magnetic field and the instability is damped.

For simplicity we assume that the stellar magnetic field $\mathbf{B}$ is initially dipolar and aligned with the star's spin axis

$$\mathbf{B}_0 = \mathbf{B}^p(t=0) = B_d \frac{R^3}{r^3}(2\,\mathtt{cos}\,\theta\,\mathbf{e}_r + \,\mathtt{sin}\,\theta\,\mathbf{e}_\theta) \tag{2.4}$$

where B_d is the strength of the equatorial magnetic field at the stellar surface. The initial magnetic field is assumed to be described by Eq. (2.4) both inside and outside. In order to avoid divergences we assume the previous radial dependence of the dipolar field to hold only for $r \geq pR$ where $1 > p > 0$. An example of a magnetic field which is dipolar in the external region and not singular at the origin is provided in [35]. Notice also that if the dipolar field remains roughly constant in the inner region its contribution to the volume averaged final toroidal field is negligible. Therefore in the following and in agreement with Ref. [6], radial integrations extend from pR to R.

To estimate the magnetic field produced by r-modes we start by writing the $l = m = 2$ contribution to the perturbation velocity (see Eq. (1.4)):

$$\delta\mathbf{v}(r,\theta,\phi,t) = \alpha\Omega R \left(\frac{r}{R}\right)^2 \mathbf{Y}^B_{22} e^{i\sigma t} \tag{2.5}$$

where $\mathbf{Y}^B_{22}$ is the magnetic-type vector spherical harmonic and σ is the frequency of the mode in the inertial frame, both defined in Chapter 1. Following Ref. [5]

we get the total azimuthal displacement from the onset of the oscillation at t_0 up to time t, which reads:

$$\begin{aligned}\Delta\tilde{x}^{\phi}(r,t) &\equiv \int_{t_0}^{t}\delta v^{\phi}(t')dt' \\ &= \frac{2}{3}\left(\frac{r}{R}\right)k_2(\theta)\int_{t_0}^{t}\alpha^2(t')\Omega(t')dt' + \mathcal{O}(\alpha^3)\end{aligned} \tag{2.6}$$

where $k_2(\theta) \equiv (1/2)^7(5!/\pi)(\mathtt{sin}^2\theta - 2\mathtt{cos}^2\theta)$. The relation between the new and the original magnetic field inside the star in the Lagrangian approach reads [5]:

$$\frac{B^j}{\rho}(\tilde{\mathbf{x}},t) = \frac{B^k}{\rho}(\mathbf{x},t_0)\frac{\partial\tilde{x_j}(t)}{\partial x^k(t_0)}. \tag{2.7}$$

This equation implies that the radial dependence of the initial and final magnetic field is the same. Integrating on time the induction equation in the Eulerian approach one gets [6]:

$$\begin{aligned}\delta B^{\theta} &\simeq \delta B^{r} \simeq 0 \\ \delta B^{\phi} &\simeq B_0^{\theta}\int\dot{\phi}(t')dt' \simeq B_0^{\theta}\int\frac{\delta v(t')}{r}dt'\end{aligned} \tag{2.8}$$

where B^{ϕ} is the toroidal component and we have set $\dot{\phi} \simeq \delta v/r$.
The rate of production of magnetic energy can be obtaining using Eqs.(2.3,2.6,2.8) and reads

$$\frac{dE_m(t)}{dt} = \left[\frac{4(1-p)}{9\pi p}\right]B_d^2R^3\Lambda'\alpha^2(t)\Omega(t)\int_0^t\alpha^2(t')\Omega(t')dt' \tag{2.9}$$

where $\Lambda' \equiv \int_0^{2\pi}d\phi\int_0^{\pi}(\kappa_2(\theta))^2|\mathbf{Y}_{22}^B(\theta,\phi)|\Psi(\theta)\mathtt{sin}\theta d\theta$ is $\mathcal{O}(1)$.

Magnetic damping

A critical point in the balance between the energy spent in producing magnetic field and the energy provided by the emission of gravitational waves is reached

when the two rates are equal

$$\frac{dE_M}{dt} = \left(\frac{d\tilde{E}}{dt}\right)_{GW} . \tag{2.10}$$

We have defined $(d\tilde{E}/dt)_{GW}$ in Chapter 1. After the balance described in (2.10) is reached, the two rates become different again, $dE_M/dt > (d\tilde{E}/dt)_{GW}$, because the toroidal magnetic field, and hence dE_M/dt, will continue to grow whereas $(d\tilde{E}/dt)_{GW}$ decreases as the emission of gravitational waves causes the star to spin down. The only source of energy to feed E_M is the energy of the mode which thus damps on a timescale

$$\tau_M = \frac{\tilde{E}}{(dE_M/dt)} . \tag{2.11}$$

The explicit expression of the magnetic damping rate $F_{m_i}(t) \equiv 1/\tau_M$ can be obtained using Eqs. (2.2,2.9):

$$F_{m_i}(t) \simeq \frac{4(1-p)}{9\pi p \cdot (8.2 \times 10^{-3})} \frac{B_p^2 R\Lambda' \int_0^t \alpha^2(t')\Omega(t')dt'}{M\Omega} \tag{2.12}$$

where the $(1-p)/p$ factor stems from the volume integral extended from pR to R. In the following, when not otherwise indicated we have used $p = 1/2$. The dependence of our results on p will be discussed later. The time integral over the r-mode amplitude α takes contributions from the period during which the star is inside the instability region.

2.2 New r-mode equations

In a magnetic star the canonical angular momentum obeys the following equation:

$$dJ_c/dt = \quad 2J_c\{F_g(M,\Omega) - [F_v(M,\Omega,T_v) + F_{m_i}(M,\Omega,B)]\} \tag{2.13}$$

where now we have also introduced the damping rate F_{m_i}, associated with the generated internal magnetic field. The total angular momentum continue to satisfy the Eq. (1.28). In the Thesis we are not considering further breaking mechanisms as e.g. the interaction between the magnetic field and the accretion disk. Combining Eqs. (2.13) and (1.28) we obtain the evolution equations of the r-mode amplitude α and of the angular velocity of the star Ω:

$$\begin{aligned}\frac{d\alpha}{dt} = \quad & \alpha(F_g - F_v - F_{m_i}) + \alpha[K_j F_g + (1-K_j)(F_v + F_{m_i})]K_c\alpha^2 \\ & -\frac{\alpha\dot{M}}{2\tilde{I}\Omega}\left(\frac{G}{MR^3}\right)^{1/2} + \frac{\alpha F_{m_e}}{2} \qquad (2.14)\\ \frac{d\Omega}{dt} = \quad & -2K_c\Omega\alpha^2[K_j F_g + (1-K_j)(F_v + F_{m_i})] \\ & -\frac{\dot{M}\Omega}{M} + \frac{\dot{M}}{\tilde{I}}\left(\frac{G}{MR^3}\right)^{1/2} - \Omega F_{m_e} \qquad (2.15)\end{aligned}$$

where we use again the notation $I_* = \tilde{I}MR^2$ with $\tilde{I} = 0.261$ for an n=1 polytrope and $K_c = 9.4 \times 10^{-2}$, see Ref. [14]. Our results turn out to be rather insensitive to the value of $K_j \sim 1$ (see Ref. [20]).

In the next Chapter we analyze the evolution of the r-modes and of the generated magnetic fields by solving numerically Eqs. (1.25,2.12,2.14,2.15).

Chapter 3

Evolution of the r-modes in millisecond pulsars

In Chapter 1 we have shown how r-mode instability plays a very important role in the evolution of the fastest spinning pulsars. In particular the rotation of recycled pulsars may be limited by the emission of gravitational radiation induced by r-modes.

In this Chapter we consider a scenario with a normal neutron star without a crust and we take into account the interaction between internal magnetic fields and r-modes by solving numerically the Eqs. (1.25,2.12,2.14,2.15).

In the following we investigate how the generation of huge internal magnetic fields influence the development of the instability both in accreting and in hot, young millisecond pulsars.

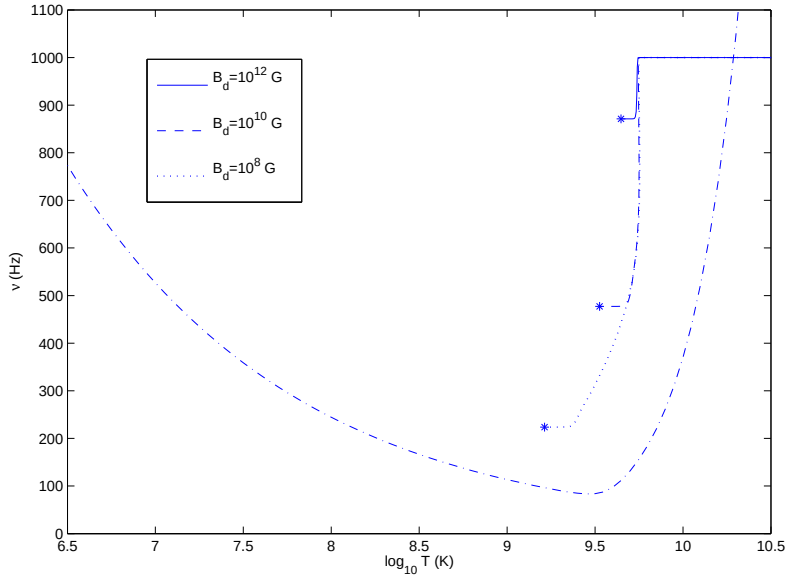

Figure 3.1: Trajectories of hot, newly born neutron stars in the $T-\nu$ plane. We indicate with asterisks the moment at which the generated toroidal magnetic fields damp the r-modes. We consider an initial spin frequency $\nu = 1000$ Hz and three different values of the initial dipolar magnetic field $B_d = (10^8, 10^{10}, 10^{12})$ G. We have chosen an r-mode saturation amplitude $\alpha_s = 1$.

3.1 Newly born millisecond pulsars

In this Section we investigate the generation of internal magnetic fields in hot, newly born neutron stars. When the star enters the instability region, the r-modes grow exponentially and generate a differential rotation which greatly amplify a pre-existent poloidal magnetic field, generating in such way a strong toroidal field. Unlike the case of non-magnetic stars (see Chapter 1), the energy of the modes is transferred to the magnetic field and the instability is damped before the star loses most of its angular momentum.

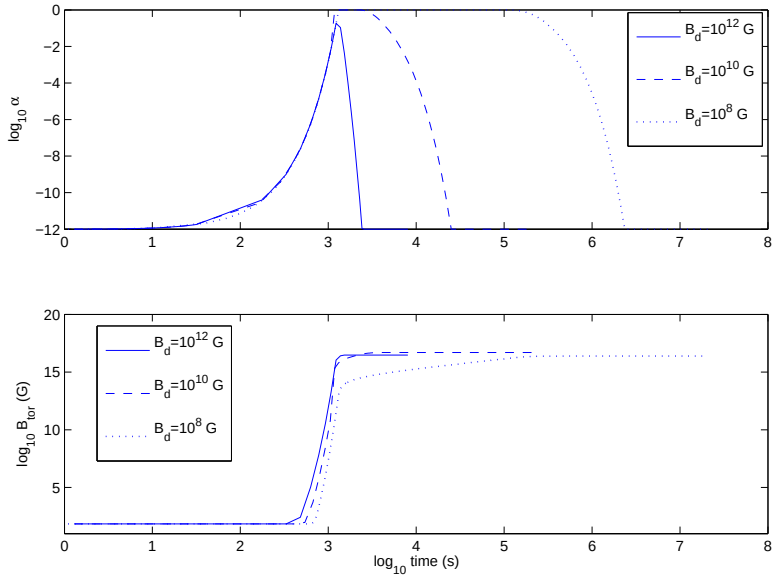

Figure 3.2: Upper panel: evolution of the r-mode amplitude for a hot, newly born neutron star. In the cases $B_d = (10^8, 10^{10})$ G, it reaches the saturation value $\alpha_s = 1$. Bottom panel: evolution of the internal toroidal field generated by r-modes. In all the cases we have considered, toroidal fields reach a value $B_{tor} \gtrsim 10^{16}$ G.

In Fig. (3.1) we show the trajectory of a newly born magnetic star in the instability window, obtained by solving numerically Eqs. (1.25,2.12,2.14,2.15). We consider an initial spin frequency $\nu = 1000$ Hz and we indicate with asterisks the moment at which the generated fields damp r-modes. In Fig. (3.2) we show the evolution of the internal magnetic fields and of the r-mode amplitude α. We have assumed a saturation value $\alpha_s = 1$. We consider three initial values of dipolar magnetic fields $B_d = (10^8, 10^{10}, 10^{12})$ G. In all the evaluated cases we have obtained the generation of huge toroidal fields, $B_{tor} \gtrsim 10^{16}$ G. These results are in agreement with conclusion of Ref. [5, 6].

If the generated internal fields exceed the critical value of the magnetic buoyancy, that in an early stage of the formation of the neutron star is a percent or less [36] of the final value $B_{buoy} \sim 10^{17}$ G of a stable stratified star [37], it can float to the surface. This happens because a strong field reduces the gas pressure and density in it, so that loops of the azimuthal field tend to float upward against the direction of gravity [36].

R-mode instability, therefore, can provide a valid mechanism to generate the strong magnetic fields observed in high magnetized stars, $B \sim (10^{14}$–10^{15} G), the so called "magnetar", that several authors [38, 39, 40] in the last years have indicated as a possible central engine of the Gamma Ray Bursts (GRBs).

3.2 Accreting millisecond pulsars in LMXBs

We consider a scenario in which the mass accretion spins an initially slowly rotating neutron star up to millisecond period and we investigate the evolution of internal toroidal magnetic fields when the star enters the r-modes instability window.

We start by discussing the evolution of temperature and spin frequency obtained without magnetic fields, already introduced in the Chapter 1. In Fig. 3.3 we show that the star crosses the r-mode instability region in a regime of thermo-gravitational runaway [22]. R-modes grow exponentially due to the decrease of the shear viscosity with increasing temperature. As a consequence r-mode amplitudes rapidly reach the saturation value (we chose $\alpha_{sat} = 1$ although, as we shall see later, magnetic fields limit $\alpha \ll \alpha_{sat}$) and the viscosity heats significantly the star. At this stage the star loses angular momentum by emission of gravitational

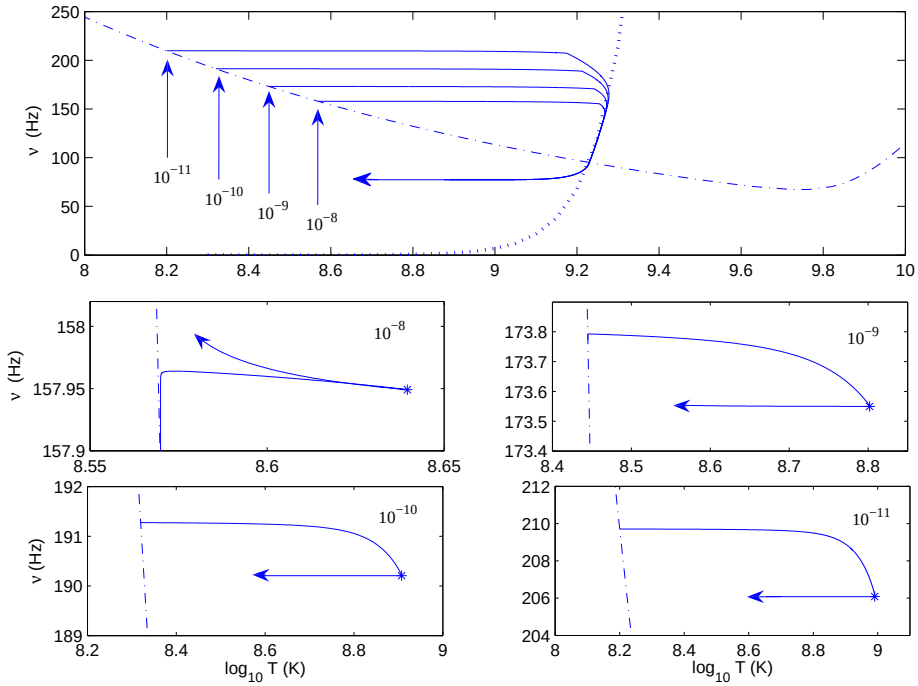

Figure 3.3: Top panel: instability region in the Temperature vs Frequency plane obtained using the shear viscosity damping rate F_ν given in [11] and the bulk viscosity damping rate F_b given in [14] (region above the dashed line). Also shown are the paths followed by accreting neutron stars, without toroidal magnetic fields (solid lines). The four curves correspond to different values of accretion rate $\dot{M} = (10^{-8}, 10^{-9}, 10^{-10}, 10^{-11})$ $M_\odot$ yr^{-1}. We plot also the temperature equilibrium curve [22] (dotted line), obtained taking into account the neutrino cooling and the reheating due to viscosity. Bottom panels: new paths obtained taking into account the new generated toroidal fields. Here $B_d = 10^8$ G. The moments at which toroidal magnetic fields damp r-mode instabilities are indicated by asterisks.

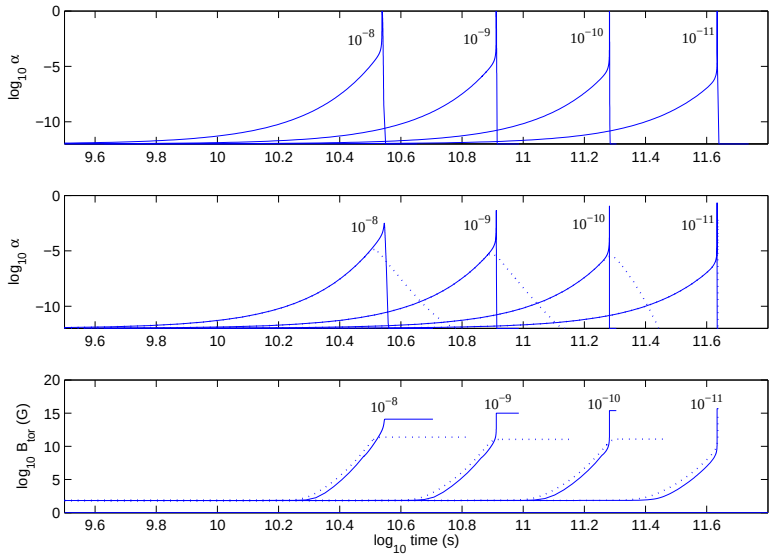

Figure 3.4: Top panel: temporal evolution of r-modes amplitude without toroidal fields. Middle panel: temporal evolution of r-modes amplitude with toroidal fields for $B_d = 10^8$ G (solid line) and $B_d = 10^9$ G (dotted line). Bottom panel: temporal evolution of volume averaged toroidal magnetic fields. We consider $\dot{M} = (10^{-8}, 10^{-9}, 10^{-10}, 10^{-11})$ $M_\odot$ yr^{-1}.

waves and goes out of the instability region in a time of hundred of years.

Taking into account magnetic fields, the evolutionary scenario for the star is quite different. We discuss results obtained solving in a self-consistent way Eqs. (1.25,2.12,2.14,2.15). From a practical viewpoint we proceed as follows: we first solve Eqs. (1.25,2.14,2.15) and we get an estimate of $F_{m_i}(t)$ inserting the results in Eq. (2.12); we use this estimate to solve again Eqs. (2.14,2.15,1.25). This procedure is iterated till numerical convergence is reached.

The exponential growth of r-modes induces extremely large secular effects and

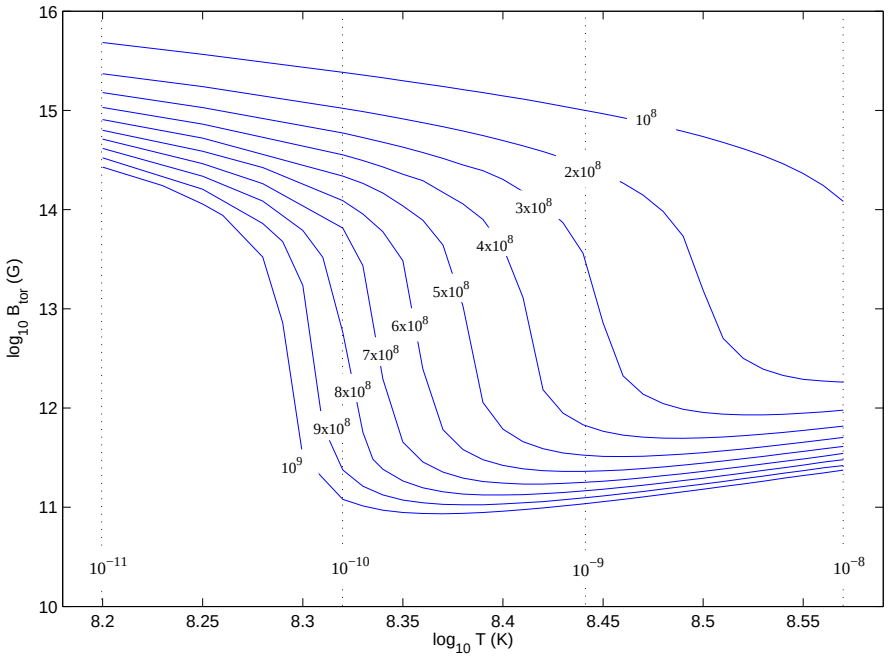

Figure 3.5: Volume averaged toroidal magnetic field generated by r-modes as a function of the temperature at which the star enters the instability window. For reference we show also the value of the temperatures which correspond to a mass accretion rate $\dot{M} = (10^{-8}, 10^{-9}, 10^{-10}, 10^{-11})$ $M_\odot$ yr^{-1}. The various curves correspond to different values of the initial poloidal magnetic field, in the range $[10^8 - 10^9]$ G. Here $p = 0.5$.

the toroidal magnetic field is either produced or amplified by the wrapping of the poloidal field produced by the secular velocity field which is mostly toroidal. In the bottom panel of Fig. 3.3 we show the new trajectory of the star in the Temperature-Frequency plane obtained taking into account the generated toroidal fields, and we indicate with asterisks the moments at which magnetic fields damp r-modes. It is important to remark that this happens when the star is still in the region which was unstable taking into account only the viscous damping.

In Fig. 3.4 we show the evolution of the r-mode amplitude α, without magnetic field (top panel) and with magnetic field (middle panel). Four different values of accretion rate $\dot{M}$ and two values of the initial poloidal magnetic field B_d are considered. In the scenario with magnetic fields, the maximum values of α are in the range $\alpha_{max} \sim [10^{-6} - 10^{-1}]$ and the generated toroidal fields are in the range $B_{tor} \sim [10^{11} - 10^{15}]$ G (Fig. 3.4 bottom panel). Here and in the following we display magnetic fields averaged on a volume which corresponds to the integration region. In this analysis we have considered values of accretion rate $\dot{M}$ and magnetic field B_d typical of accreting Low Mass X-Ray binaries (LMXBs). As indicated in Table 1 of Ref. [41] the values of $\dot{M}$ for LMXBs are in the range $(10^{-8} - 10^{-11})\mathrm{M}_{\odot}\mathrm{yr}^{-1}$.

In Fig. 3.5 we show the generated toroidal magnetic field as a function of the temperature at which the star enters the instability window. We display the volume averaged field obtained at the moment in which the field itself has completely damped r-modes. The value of the magnetic field is the asymptotic one displayed in the bottom panel of Fig. 3.4. Results of Fig. 3.5 are obtained using Eqs. (1.22,1.23) to describe the connection between accretion rate $\dot{M}$ and temperature T. To better understand the dependence of our results on the relation

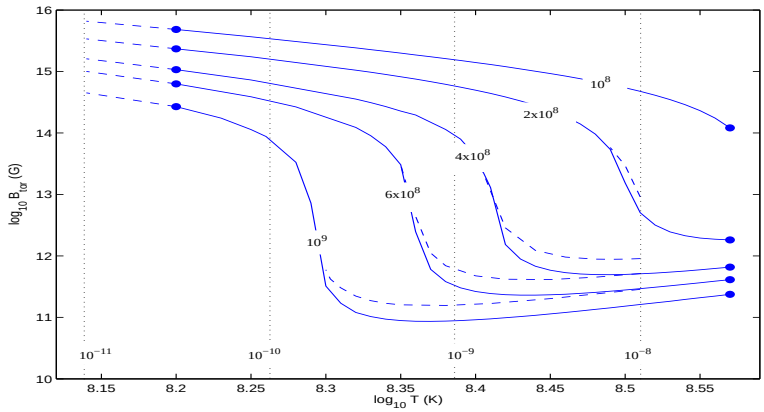

Figure 3.6: Same as Fig. 3.5. Here the solid lines are obtained taking into account also the reheating term $\dot{\epsilon}_h$ (Eq. (1.23)), while the dashed lines are obtained neglecting that contribution.

between mass accretion rate and temperature, in Fig. 3.6 we compare the final toroidal fields obtained taking into account both contributions to accretion heating described in Eqs. (1.22,1.23) with the fields obtained neglecting the second contribution i.e. $\dot{\epsilon}_h$. If $\dot{\epsilon}_h$ is neglected then temperature is lower for a same value of $\dot{M}$ and a general outcome of our analysis is that the toroidal fields are larger. Finally, our results depend on the extension of the region of integration in Eq. 2.12, which also corresponds to the region inside the star where the initial magnetic field and the r-modes are both sizable. The dependence of the generated toroidal fields on p is shown in Fig. 3.7. It is clear that the scenario we are obtaining is not too dependent on p.

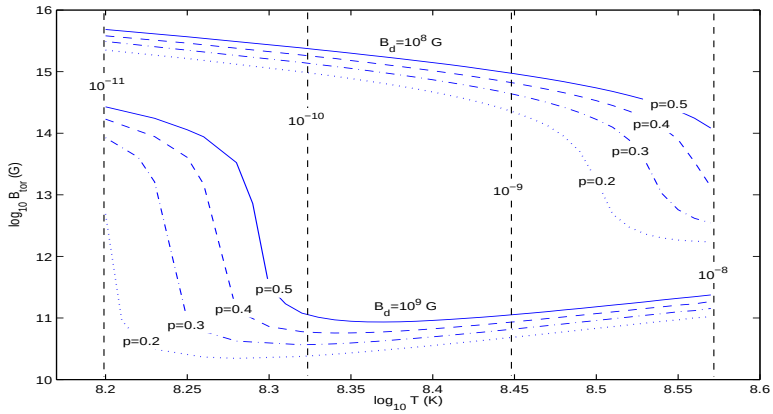

Figure 3.7: Same as Fig.3.5. The different lines correspond to different values of the integration volume, indicated by different values of p. Two values of initial magnetic field are considered.

3.3 Instability and evolution of magnetic fields

Several issues remain open concerning how the new generated magnetic fields are affected by possible instabilities. In the stably stratified environment of a stellar interior there are two types of instabilities: the Parker (or magnetic buoyancy) and the Tayler instabilities (or pinch-type), both driven by the magnetic field energy in the toroidal field. The buoyancy instability is negligible for $B_{tor} \lesssim 10^{17}$ G [37], so we focus on Tayler instabilities because they set in at a lower field strength [42]. It is important to remark that in a stable and stratified neutron star the condition for the Tayler instability reads [43]:

$$\frac{\omega_A}{\Omega} > \left(\frac{N_\mu}{\Omega}\right)^{1/2} \left(\frac{\eta}{r^2\Omega}\right)^{1/4} \tag{3.1}$$

where $\omega_A = B/(4\pi\rho)^{1/2}r$ is the Alfvén frequency, $N_\mu \simeq 5 \times 10^4$ s^{-1} is the compositional contribution to the buoyancy frequency and $\eta \sim 10^{-9}$ cm^2 s^{-1} is the

magnetic diffusivity which can be obtained from the electrical conductivity σ (given in [44]) by using the relation $\eta = 1/(\mu_0\sigma)$. From Eq. (3.1) we can conclude that in the stably stratified core of a neutron star, the Tayler instability sets in for $B_{tor}^{cr} \gtrsim 10^{12}$ G.

After the development of the Tayler instability, the toroidal component of the field produces, as a result of its decay, a new poloidal component which can then be wound up itself, closing the dynamo loop. Both components then grow, more slowly, until the saturation level is reached, when the field is being destroyed by the instability at the same rate at which it is being amplified by the differential rotation [45]. When the differential rotation stops the field can evolve into a stable configuration of a mixed poloidal-toroidal twisted-torus shape embedded inside the star with an approximately dipolar field connected to it outside the star [46, 47, 48, 49].

Once the field is stabilized it should evolve as a result of diffusive processes as Ohmic dissipation, ambipolar diffusion, and Hall drift [50], whose typical time-scales are:

$$t_{ohmic} \sim 2 \times 10^{11} \frac{L_5^2}{T_8^2} \left(\frac{\rho}{\rho_{nuc}}\right)^3 \text{ yr} \tag{3.2}$$

$$t_{ambip} \sim 3 \times 10^{9} \frac{T_8^2 L_5^2}{B_{12}^2} \text{ yr} \tag{3.3}$$

$$t_{Hall} \sim 5 \times 10^{8} \frac{L_5^2}{B_{12}} \left(\frac{\rho}{\rho_{nuc}}\right) \text{ yr} \tag{3.4}$$

where $L_5 = L/10^5$ cm is the size of the region embedding the magnetic field.

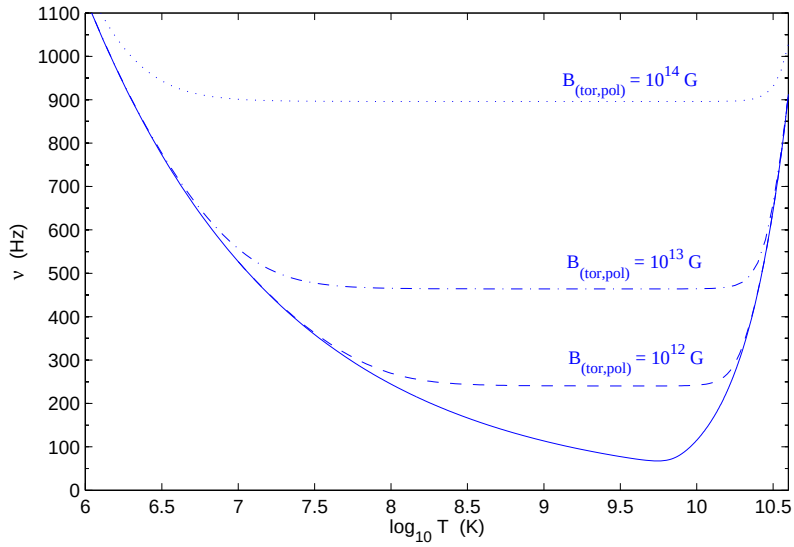

Figure 3.8: New r-modes instability regions for neutron stars with stable configurations of mixed poloidal-toroidal fields in the inner core (no magnetic field - solid line; $B_{tor,pol} = 10^{12}$ G - dashed line; $B_{tor,pol} = 10^{13}$ G - dotted-dashed line; $B_{tor,pol} = 10^{14}$ G - dotted line). We assume that poloidal and toroidal components have similar strengths.

3.4 Internal magnetic fields and new r-mode instability windows

We have shown how r-modes can generate strong toroidal fields in the core of accreting millisecond neutron stars, and how these fields influence the growth rate of r-mode instabilities. Tayler instability sets in for strengths of the generated fields of the order of 10^{12} G and stabilizes the toroidal component by producing a new poloidal field of similar strength. This stable configuration evolves on a time-scale, regulated by diffusive processes. Our results imply that in the core of accreting neutron stars in LMXBs, rotating at frequencies $\nu \gtrsim 200$ Hz, there are

strong magnetic fields with strengths $B \gtrsim 10^{12}$ G.
Finally, it is tempting to try to investigate how the new stable configuration of magnetic fields modifies the instability window of r-modes. More explicitly the scenario we have in mind is the following:

- the compact star inside the LMXB initially enters the instability window and it follows the trajectories that are displayed in the bottom panel of Fig. 3.3 and in Fig. 3.4. When the toroidal field reaches the critical value dictated by the Tayler instability, the poloidal field suddenly increases and we assume it reaches a value of the same order of B_{tor}^{cr}. The new magnetic configuration, in which the poloidal and the toroidal field are of the same order of magnitude, is stable. In the new configuration the internal poloidal field is a few orders of magnitude larger than the initial poloidal field. R-modes try again to deform the poloidal field generating a new toroidal component but the magnetic damping rate given by Eq. (2.12) is now much larger and the star is stable with respect to r-modes up to frequencies of the order of 200 Hz.

- the star continues accreting and increasing its frequency and it enters again the instability region generating again a new toroidal field. When the new toroidal component becomes much larger than the poloidal component Tayler instability sets in again increasing the value of the poloidal field. In Fig. 3.8 we show how the instability window changes in dependence of the internal magnetic configuration, assuming that the toroidal and poloidal components are equal.

- to determine the actual maximum value of the limiting frequency we take

into account also the time-scale associated with the diffusive processes described by Eqs.(3.2–3.4). If the magnetic fields exceed a few 10^{14} G the diffusion time-scale becomes shorter than 10^6 yr and the star cannot accelerate further even for very large values of $\dot{M}$.

It is clear that even in the absence of the Ekman layer the new internal magnetic fields can stabilize stars with frequencies up to several hundreds Hertz. The possible presence of a superconducting shell would screen these internal fields so that they would not affect the dynamics of the external region.

3.5 Open problems

In our work we have not discussed the possible existence of Ekman layer. As discussed in Chapter 1, if this layer is present it can stabilize the star up to frequencies of a few hundred Hertz. The scenario discussed above does not change qualitatively, but since the star enters the instability region at higher frequencies, the growth rate of magnetic fields is larger.

Another important open point concerns the possible formation of superconductivity in the core of neutron stars. A fraction of the core, whose temperature is below the critical value $T_c \sim 10^9$ K, is expected to be either a Type I [52, 53] or a Type II superconductor [51, 54]. The exact nature of the possible superconducting layer is still uncertain as well as the precise value of the superconducting gap. Microscopically, the only gap associated with protons which has been evaluated is the $^1S_0$ [55, 56, 51]. The fundamental quantity in our analysis is the size of the superconducting region which we show in Fig. 3.9 using the results obtained in [51], which are compatible with previous estimates: the thickness of the super-

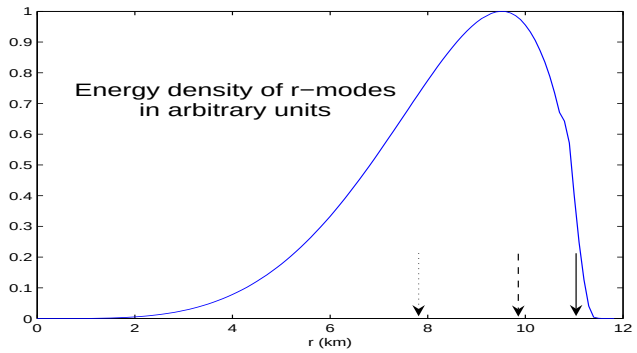

Figure 3.9: Energy density of r-modes as a function of the star radius. Also indicated is the region where superconductivity can form. The estimates about the size of the superconducting region are quite uncertain. The solid arrow indicates the external border of the superconducting region, the dashed and the dotted arrows indicate two possible locations of the internal border obtained from [51].

conducting shell is about (1–3) km.

The $^3PF_2$ pairing of neutrons and protons is still affected by many theoretical uncertainties. The $^3PF_2$ pairing of neutrons has been evaluated in [57, 55] and, together with $^1S_0$ gap it contributes to the neutron superfluidity. In our analysis we have taken into account the effect of superfluidity on viscosity, see Eq. (1.16). In the same figure we also display the energy density of the r-modes. It is clear that a large fraction of the volume where r-modes can develop remains not superconducting and in that region our analysis can still be applied: r-modes are damped by the magnetic field and therefore the perturbation velocity drops to zero. In Fig. 3.10 we show that in the not superconducting region large magnetic fields will form and they are large enough to damp r-mode oscillations. The integration region extends from pR to p_1R, where p_1R corresponds to the inner

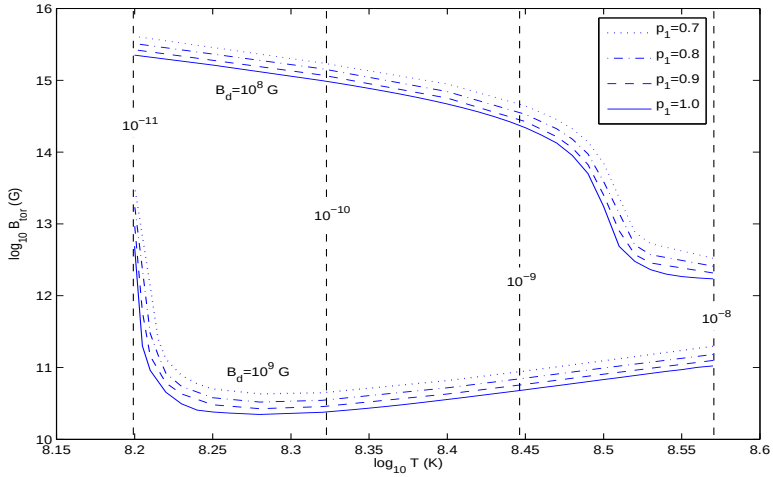

Figure 3.10: Same as Fig. 3.5. Here the integration region extends from pR to $p_1 R$, and we assume $p = 0.2$.

border of the superconducting region. R-modes can develop in the superconducting layer, but their amplitude is strongly suppressed because the perturbation velocity has to vanish at the interface between the superconducting and the not superconducting region. Moreover, if the superconductivity is of Type II, the magnetic flux of the original poloidal field organizes into quantized flux tubes. R-modes will stretch these flux tubes, increasing their length and thus changing their magnetic energy content. As in the case of the normal core, this process can generate very intense magnetic fields which lead to the damping of the r-mode oscillations even in the superconducting layer [6].

Chapter 4

Astrophysical scenarios

In this Chapter we analyze the astrophysical implications of our results. As we have shown previously, r-mode instability can generate huge magnetic fields in the core of millisecond neutron stars. In turn, the so-generated magnetic fields can stabilize the millisecond pulsars at high spin frequencies.
In the next section we first consider the case of LMXBs and we try to understand whether and under which conditions, in our scenario, the emission of gravitational waves limits the spin frequencies of the rapidly rotating neutron stars. We then follow the spin frequency evolution of millisecond pulsars when mass accretion stops, in order to understand whether the emission of gravitational waves plays also a role in the spin down of these objects.

4.1 Spin frequencies evolution of LMXBs

In the scenario we are analyzing, the evolution of the internal magnetic field drives the evolution of the spin frequency of the star when the star is in the region

which was unstable taking into account only the viscous damping. Internal magnetic fields evolve due the diffusive processes discussed previously (Ohmic dissipation, ambipolar diffusion and Hall drift) on timescales given by Eqs. (3.2,3.3,3.4). When the magnetic field decreases, the instability region changes (see Fig. 3.8) and the star becomes again unstable with respect to r-modes and it spins down by emission of gravitational waves. At the same time, the development of the instability generates a new toroidal field that stabilizes again the star.
This scenario can take place through two different paths:

- the spin down of the star is discontinuous: the diffusion of the internal magnetic field makes the star unstable with respect to r-modes; the star loses angular momentum by emission of gravitational waves; the instability generates a new toroidal field that stabilizes again the star; the generated field is again dissipated and the star is newly unstable, and so on.

- the star is constantly in the instability region with a tiny value of the r-mode amplitude α; the dissipation of the internal magnetic fields is slowed due to the continuous formation of "new" fields.

In both scenarios, the partial regeneration of the magnetic field when the star becomes unstable with respect to r-modes, slightly reduces the diffusion of the internal field on the long time scale. However this effect is difficult to estimate and in the following we neglect it.
In the following, in addition to mass accretion and internal magnetic field, we take into account also of the magnetic dipole emission of the star, and we neglect other spin down mechanisms, e.g. the interaction between the accretion disk and the external magnetic field, in order to better understand the effect of the emis-

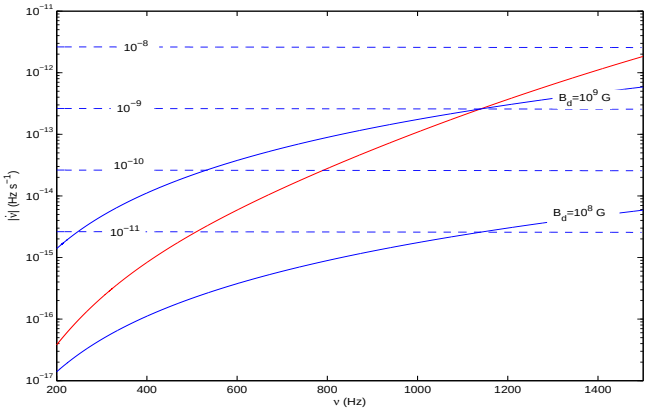

Figure 4.1: The solid red line identify the absolute value of the spin frequency derivative $|\dot{\nu}_{GW}|$ associated with the emission of gravitational wave. Blue solid lines identify the absolute value of the spin frequency derivative $|\dot{\nu}_B|$ associated with the dipole emission; we consider two values of external magnetic field $B = (10^8, 10^9)$ G. The dashed lines identify the absolute value of the spin frequency derivative $|\dot{\nu}_{MA}|$ associated with the mass accretion; we consider four values of mass accretion rate $\dot{M} = (10^{-8}, 10^{-9}, 10^{-10}, 10^{-11})\,\mathrm{M}_\odot\mathrm{yr}^{-1}$.

sion of gravitational waves on the spin frequency evolution of millisecond pulsars.

In Fig. 4.1 we show the absolute values of the possible spin frequency derivative $|\dot{\nu}|$ due to: the mass accretion (dashed lines, $\dot{\nu}_{MA} > 0$); the emission of gravitational waves (red line, $\dot{\nu}_{GW} < 0$) and the dipole emission (blue solid lines, $\dot{\nu}_B < 0$). Results are plotted in a ν–$\dot{\nu}$ plane. The spin frequency derivative $\dot{\nu}_{GW}$ is obtained by taking into account the emission of gravitational waves due to the dissipation of the internal magnetic fields. Due to the dependence of the dissipation timescales on the temperature, this curve changes by changing the value of the mass accretion rate $\dot{M}$. Clearly the emission of gravitational waves and the

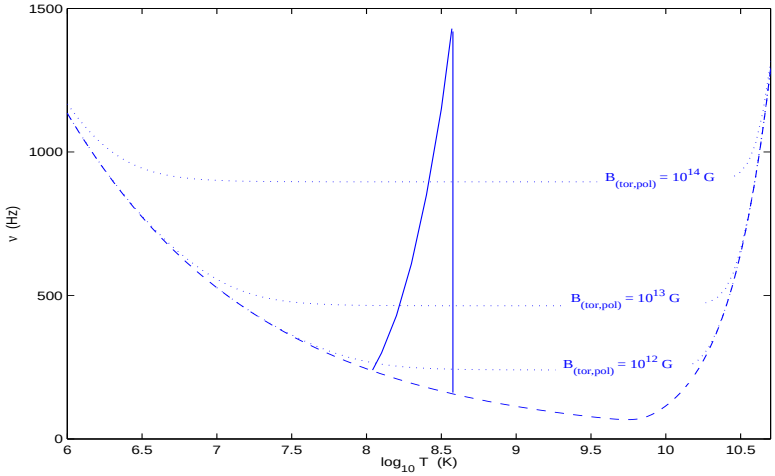

Figure 4.2: The solid line is obtained by the condition $|\dot{\nu}_{MA}| = |\dot{\nu}_{GW}|$. It represents the maximum spin frequency at which it is possible to accelerate a star at fixed $\dot{M}$. We make use of Eqs.(1.22,1.23) for the relation between the temperature T and the mass accretion rate $\dot{M}$.

dipole emission spin down the star, so $\dot{\nu}_{GW}$ e $\dot{\nu}_B$ are negative quantities; on the contrary the mass accretion increases the spin frequency of the star, so $\dot{\nu}_{MA}$ is a positive quantity.

With reference to Fig. 4.1, at fixed $\dot{M}$, the condition $|\dot{\nu}_{MA}| = |\dot{\nu}_{GW}|$ or $|\dot{\nu}_{MA}| = |\dot{\nu}_B|$ returns the maximum spin frequency at which it is possible to accelerate a star for that value of mass accretion. For magnetic fields in the range (10^8–10^9) G, which are typical values for LMXBs, above $\nu \sim 900$ Hz the millisecond accreting pulsars are limited by the emission of gravitational waves because $|\dot{\nu}_{GW}| > |\dot{\nu}_B|$. Below $\nu \sim 900$ Hz the dipole emission is relevant only for values of the external magnetic field $B \gtrsim 5 \times 10^8$ G. If $|\dot{\nu}_B| > |\dot{\nu}_{GW}|$ the star departs from the edge of the instability region and it spins down by dipole emission.

In Fig. 4.2 we make use of the results of Fig. 4.1 and we show how r-modes limit the spin frequencies of the accreting millisecond pulsars in the T–ν plane. Stable accreting neutron stars can be accelerate up to the solid line, where $|\dot{\nu}_{MA}| = |\dot{\nu}_{GW}|$. In the same figure we plot also the values of the internal fields as a function of the spin frequency (see also Fig. 3.8), and the region that was unstable taking into account only the viscosity. In the scenario we are considering, a star can reach frequencies $\nu \gtrsim 1000$ Hz only if it accretes a mass $\gtrsim 0.1\,\mathrm{M}_\odot$ at a stable accretion rate $\dot{M} \sim 10^{-8}\,\mathrm{M}_\odot\,\mathrm{yr}^{-1}$. In the other cases the emission of gravitational waves should limit the spin frequency of accreting neutron stars at $\nu \lesssim 1000$ Hz.

4.2 Connection between LMXBs and millisecond radio pulsars

Millisecond pulsars are commonly believed to be descendants of normal neutron stars that have been spun-up and recycled back as radio pulsars by acquiring angular momentum from their companion during the Low-mass X-ray binary phase. Towards the end of the secular LMXB evolution, as accretion rate fall below a critical value, above which the radio emission may be hampered due to absorption or dispersion [58], the neutron star can re-appear as a MSRP. In the standard spin-down model, the MSRP evolution is driven by pure magnetic dipole radiation. Alternative energy loss mechanisms such as multipole radiation or gravitational wave emission, especially during the initial phases of the reborn millisecond pulsars, have been suggested by several authors [26, 59]. A recent statistical analysis [60] tries to obtain the spin frequency distribution of MSRPs starting by the spin frequency distribution of MSXPs. However it is able to re-

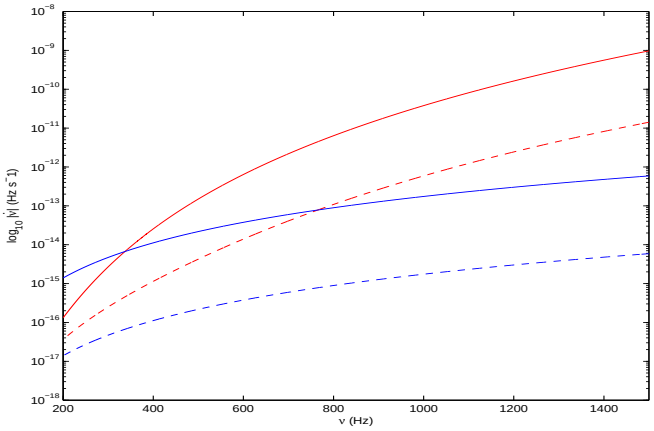

Figure 4.3: As Fig. 4.1. The solid red line is related to the emission of gravitational waves for stars whose temperature is $T = 10^7$ K; the dashed red line is obtained for $T = 10^8$ K. For comparison we plot also the spin frequency derivative due only to the dipole emission: $B = 10^8$ G (dashed blue line), $B = 10^9$ G (solid blue line).

produce only the general demography of older MSRPs, while it fails to predict the younger and fastest MSRP sub-population. A possible explanation proposed in Ref. [60] is that the standard evolutionary model fails because the MSRPs, during some portion of their evolution, lose energy through a dominant mechanism other than magnetic dipole radiation.

In order to understand if the emission of gravitational waves can play a role in the evolution of the fastest MSRPs, we investigate how, in our scenario, the spin frequency evolves when mass accretion stops ($\dot{\nu}_{MA} = 0$).

In Fig. 4.3 we plot the absolute values of the derivative of the spin frequency, obtained by considering the emission of gravitational waves (red lines, $\dot{\nu}_{GW}$) for two values of temperature $T = (10^7, 10^8)$ K. For comparison we plot also the spin frequency derivative of the dipole emission for two values of magnetic field

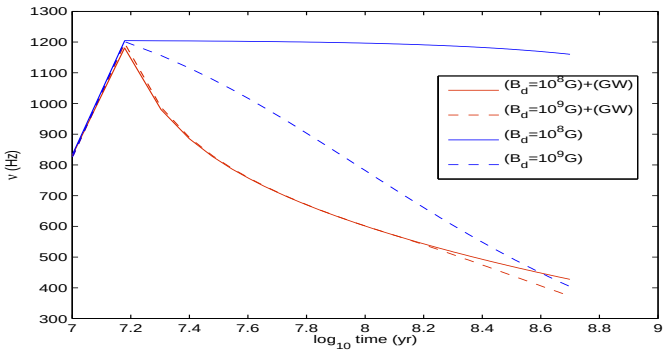

Figure 4.4: Spin frequency evolution for a neutron star accelerated at spin frequencies $\nu \sim$ 1200 Hz. We take into account the cooling rate due to the neutrino emission, the emission of gravitational waves and the dipole emission. We consider two values of the external magnetic fields, $B = (10^8, 10^9)$ G. For comparison we plot also the spin frequencies evolution obtained considering only the dipole emission (blue lines).

$B = (10^8, 10^9)$ G (blue solid lines, $\dot{\nu}_B$). Results are plotted in a ν–$\dot{\nu}$ plane. Fig. 4.3 can be interpreted as follows: if $|\dot{\nu}_{GW}|$ is greater than $|\dot{\nu}_B|$, the star loses most of its angular momentum by emission of gravitational waves. Contrary, if $|\dot{\nu}_B| > |\dot{\nu}_{GW}|$ the star spins down only by dipolar emission and it moves away from the edge of the r-mode instability window.

In Fig. 4.4 we plot the spin frequency evolution for a neutron star accelerated at frequencies $\nu \sim 1200$ Hz. We follow the spin frequency evolution by taking into account the variation of temperature due to the neutrino emission, the emission of gravitational waves and the dipole emission. We consider two values of the external magnetic field, $B = (10^8, 10^9)$ G. For comparison we plot also the spin frequency evolution obtained considering only the dipole emission (blue line). It

is evident that for frequencies $\nu \gtrsim 500$ Hz, the star loses most of its angular momentum by emission of gravitational waves. At lower frequencies the spin down can be influenced by the dipole emission.

In conclusion, the emission of gravitational waves can play a very important role in the spin down of the fastest MSRPs. Our analysis shows that the r-mode instability condition depends on the frequency, the temperature and the external magnetic field of the star (see Fig. 4.3).

Conclusions and Outlook

In this Thesis we have studied the interaction between magnetic fields and r-mode instability in millisecond pulsars. The aim of the work was to investigate this interaction in accreting stars that are spun up to millisecond period by the mass accretion. The main results obtained are the following:

- We have obtained new evolution equations for the r-mode instability by introducing for the first time the magnetic damping rate F_{m_i};
- The differential rotation induced by the r-mode instability generates huge toroidal magnetic fields both in a hot, newly born star and in old accreting stars;
- In accreting millisecond pulsars, the generated toroidal fields are stabilized by the Tayler instability. The presence of stable magnetic fields in the core of accreting stars stabilizes the star with respect to r-modes;
- given a constant value for the mass accretion rate, the maximum spin frequency is related to the value of the internal magnetic field;
- a new spin down mechanism for millisecond pulsars has been found, associated with the slow diffusion of the internal magnetic field. The dacay of

the internal magnetic field makes the star unstable again with respect to r-modes.

Finally, the work discussed in this Thesis can be extended in several directions:

- a new evolutionary path connecting LMXBs and MSRPs can be investigated, based on the existence of two mechanisms for spin down;
- the extremely large magnetic fields generated by a rapidly-rotating newly-born compact star can be relevant in the discussion of certain features of Gamma Ray Bursts, which can be explained if a magnetar is formed in the early stage of the life of the compact star.

Bibliography

[1] J. Papaloizou and J. E. Pringle, Mon. Not. Roy. Astron. Soc. **182**, 423 (1978).

[2] N. Andersson, Astrophys. J. **502**, 708 (1998).

[3] J. L. Friedman and S. M. Morsink, Astrophys. J. **502**, 714 (1998).

[4] L. Rezzolla, F. K. Lamb, and S. L. Shapiro, Astrophys. J. **531**, L141 (2000).

[5] L. Rezzolla, F. K. Lamb, D. Markovic, and S. L. Shapiro, Phys. Rev. **D64**, 104013 (2001).

[6] L. Rezzolla, F. K. Lamb, D. Markovic, and S. L. Shapiro, Phys. Rev. **D64**, 104014 (2001).

[7] S. Chandrasekhar, Phys. Rev. Lett. **24**, 611 (1970).

[8] J. L. Friedman and B. F. Schutz, Astrophys. J. **221**, 937 (1978).

[9] J. L. Friedman and B. F. Schutz, Astrophys. J. **222**, 281 (1978).

[10] J. L. Friedman, Commun. Math. Phys. **62**, 247 (1978).

[11] N. Andersson and K. D. Kokkotas, Int. J. Mod. Phys. **D10**, 381 (2001).

[12] J. Provost, G. Berthomieu, and A. Rocca, Astron. Astrophys. **94**, 126 (1981).

[13] L. Lindblom, B. J. Owen, and S. M. Morsink, Phys. Rev. Lett. **80**, 4843 (1998).

[14] B. J. Owen *et al.*, Phys. Rev. **D58**, 084020 (1998).

[15] S. L. Shapiro and S. A. Teukolsky, New York, USA: Wiley (1983) 645 p.

[16] D. Blaschke, H. Grigorian, and D. N. Voskresensky, Astron. Astrophys. **424**, 979 (2004).

[17] P. Haensel and R. Schaeffer, Phys. Rev. **D45**, 4708 (1992).

[18] T. Klähn *et al.*, Phys. Rev. **C74**, 035802 (2006).

[19] A. L. Watts and N. Andersson, Mon. Not. Roy. Astron. Soc. **333**, 943 (2002).

[20] R. V. Wagoner, Astrophys. J. **578**, L63 (2002).

[21] N. Andersson, D. I. Jones, and K. D. Kokkotas, Mon. Not. Roy. Astron. Soc. **337**, 1224 (2002).

[22] R. Bondarescu, S. A. Teukolsky, and I. Wasserman, Phys. Rev. **D76**, 064019 (2007).

[23] J. L. Friedman, L. Parker, and J. R. Ipser, Phys. Rev. Lett. **62**, 3015 (1989).

[24] P. Haensel and J. L. Zdunik, Nature **340**, 617 (1989).

[25] N. Andersson, K. D. Kokkotas, and N. Stergioulas, Astrophys. J. **516**, 307 (1999).

[26] L. Bildsten, Astrophys. J. **501**, L89 (1998).

[27] K. Glampedakis and N. Andersson, Mon. Not. Roy. Astron. Soc. **371**, 1311 (2006).

[28] M. L. E. Rieutord, Astrophys. J. **550**, 443 (2001).

[29] P. Jaikumar, G. Rupak, and A. W. Steiner, Phys. Rev. **D78**, 123007 (2008).

[30] A. Drago, G. Pagliara, and I. Parenti, Astrophys. J. **678**, L117 (2008).

[31] D. Chatterjee and D. Bandyopadhyay, Phys. Rev. **D74**, 023003 (2006).

[32] J. Madsen, Phys. Rev. Lett. **85**, 4687 (2000).

[33] J. Madsen, Phys. Rev. **D46**, 3290 (1992).

[34] H. C. Spruit, (1998).

[35] V. C. A. Ferraro, Astrophys. J. **119**, 407 (1954).

[36] H. C. Spruit, AIP Conf. Proc. **983**, 391 (2008).

[37] W. Kluzniak and M. Ruderman, Astrophys. J. **505**, L113 (1997).

[38] A. Corsi and P. Meszaros, Astrophys. J. **702**, 1171 (2009), 0907.2290.

[39] Y.-H. Fan and D. Xu, Mon. Not. Roy. Astron. Soc. **372**, L19 (2006).

[40] K. Toma, K. Ioka, T. Sakamoto, and T. Nakamura, Astrophys. J. **659**, 1420 (2007).

[41] D. Galloway, Accreting neutron star spins and the equation of state, in *40 Years of Pulsars: Millisecond Pulsars, Magnetars and More*, edited by C. Bassa, Z. Wang, A. Cumming, & V. M. Kaspi, , American Institute of Physics Conference Series Vol. 983, pp. 510–518, 2008.

[42] H. C. Spruit, Astron. Astrophys. **349**, 189 (1999).

[43] H. C. Spruit, Astron. Astrophys. **381**, 923 (2002).

[44] P. Haensel, A. Y. Potekhin, and D. G. Yakovlev, New York, USA: Springer (2007) 619 p.

[45] J. Braithwaite, Astron. Astrophys. **449**, 451 (2006).

[46] A. Reisenegger, (2008).

[47] J. Braithwaite and H. C. Spruit, Astron. Astrophys. **450**, 1097 (2006).

[48] J. Braithwaite and H. C. Spruit, Nature. **431**, 819 (2004).

[49] J. Braithwaite and Å. Nordlund, Astron. Astrophys. **450**, 1077 (2006).

[50] P. Goldreich and A. Reisenegger, Astrophys. J. **395**, 250 (1992).

[51] M. Baldo and H.-J. Schulze, Phys. Rev. **C75**, 025802 (2007).

[52] B. Link, Physical Review Letters **91**, 101101 (2003).

[53] K. B. Buckley, M. A. Metlitski, and A. R. Zhitnitsky, Physical Review Letters **92**, 151102 (2004).

[54] I. Wasserman, Mon. Not. Roy. Astron. Soc. **341**, 1020 (2003).

[55] O. Elgaroy, L. Engvik, M. Hjorth-Jensen, and E. Osnes, Phys. Rev. Lett. **77**, 1428 (1996).

[56] W. Zuo *et al.*, Phys. Lett. **B595**, 44 (2004).

[57] M. Baldo, O. Elgaroey, L. Engvik, M. Hjorth-Jensen, and H. J. Schulze, Phys. Rev. **C58**, 1921 (1998).

[58] C. Thompson, R. D. Blandford, C. R. Evans, and E. S. Phinney, Astrophys. J. **422**, 304 (1994).

[59] J. H. Krolik, Astrophys. J. **373**, L69 (1991).

[60] B. Kiziltan and S. E. Thorsett, Astrophys. J. Lett. **693**, L109 (2009).